# Optical analysis of a curved-slats fixed-mirror solar concentrator by a forward ray-tracing procedure

Ramon Pujol Nadal* and Víctor Martínez Moll

Departament de Física, Universitat de les Illes Balears, ctra. de Valldemossa km 7.5, Palma de Mallorca, 07122 Illes Balears, Spain

*Corresponding author: ramon.pujol@uib.es

Received 23 July 2013; revised 22 September 2013; accepted 24 September 2013; posted 26 September 2013 (Doc. ID 10.1364/AO.52.007389); published 18 October 2013

Fixed-mirror solar concentrators (FMSCs) use a static reflector and a moving receiver. They are easily installable on building roofs. However, for high-concentration factors, several flat mirrors would be needed. If curved mirrors are used instead, high-concentration levels can be achieved, and such a solar concentrator is called a curved-slats fixed-mirror solar concentrator (CSFMSC), on which little information is available. Herein, a methodology is proposed to characterize the CSFMSC using 3D ray-tracing tools. The CSFMSC shows better optical characteristics than the FMSC, as it needs fewer reflector segments for achieving the same concentration and optical efficiency. 

*OCIS codes:* (350.6050) Solar energy; (220.1770) Concentrators; (080.2740) Geometric optical design.

http://dx.doi.org/10.1364/AO.52.007389

## 1. Introduction

Many alternatives have been proposed for producing energy in a sustainable way. Solar energy systems are among the approaches that have been intensively studied, because solar energy is clean, abundant, and free. In this context, the International Energy Agency (IEA) encourages a process that involves taking into account new technical and scientific developments, policies, and international collaborative efforts [1]. This paper relates to two action items for research entities that the IEA roadmap has defined: (i) development of solar collectors integrated into building surfaces, and (ii) development of collectors that cover the temperature range between 100°C and 250°C (which is referred to as the medium temperature range). To address these problems, it is essential to investigate new techniques to improve the energy conversion efficiency, and particularly to develop new concentration structures that have high optical efficiency.

One kind of collector that can reach high efficiencies at medium temperatures with good adaptability to urban environments is the so-called tracking receiver/stationary reflector [2]. There are mainly two designs mentioned in the literature: the stationary reflector/tracking absorber (SRTA) and the fixed-mirror solar concentrator (FMSC). The SRTA has been analyzed in several studies [3–5]. The FMSC was analyzed during the 1970s [6–9], and recently the authors of this paper presented an optical study using a ray-tracing procedure [10].

The incidence angle modifier (IAM) provides a means of determining the optical performance when the sun is not perpendicular to the collector, and it is essential in order to know the optical behavior of a solar collector. The commonly accepted model for determining the IAM for axial collectors is a biaxial model in which the angle modifier is given by the product of the components that are transverse and longitudinal to the planes of the receiver, according to the angles defined in Fig. 1. The IAM $K$ for low-concentration collectors could be factorized as $K \sim K(\theta_t, 0)K(0, \theta_l)$ [11].

1559-128X/13/307389-10$15.00/0

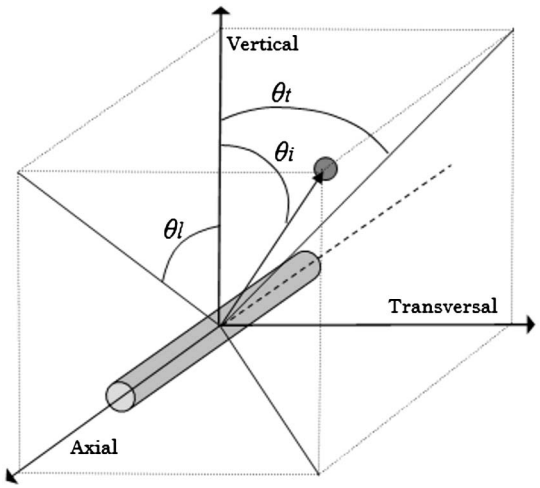


Fig. 1. $\theta_t$ and $\theta_l$ are the transverse and longitudinal angles that are the projected incidence angles on the two reference planes perpendicular to and along the axis of the collector, respectively. $\theta_i$ is the incident angle.

The aim of this paper is to analyze a modified FMSC design, called the curved-slats fixed-mirror solar concentrator (CSFMSC), with computer ray-tracing methods in order to determine the optical efficiency at normal incidence, the IAM curves, and the local flux concentration on the absorber as a function of the concentrator design parameters. The angular size of the sun, the nonuniform solar intensity distribution, and the sources of optical errors of the system were all taken into account. The IAM values are referred to the collector aperture.

## 2. Related Work

A FMSC is a mobile focus concentrator that can produce thermal energy in the medium temperature range. Due to its static reflector, the FMSC has several advantages when compared to other designs, such as being one of the best adapted for integration onto building roofs [12].

The FMSC design emerged in the 1970s as an effort to reduce electricity production costs in solar thermal power plants [6]. The FMSC consists of an arrangement of flat mirrors at different heights as shown in Fig. 2, with their respective central lines positioned along a circular path (when viewed along the axes of the mirrors) and oriented such that the rays reflected by the central points of the mirrors intersect at a point on the same base circular path. It can be easily shown that for any incident angle, the reflected rays of the central lines of the mirrors will always intersect at a unique focus on the base circle and, therefore, it would be possible to track the sun simply by positioning the receiver at a certain angle over the circular path without moving the reflector, as can be seen in Fig. 2.

An optical analysis of the FMSC was conducted using 3D ray-tracing tools [10], with the FMSC geometry defined using three parameters: the number of mirrors $N$, the F-number $(f/)$ of the concentrator

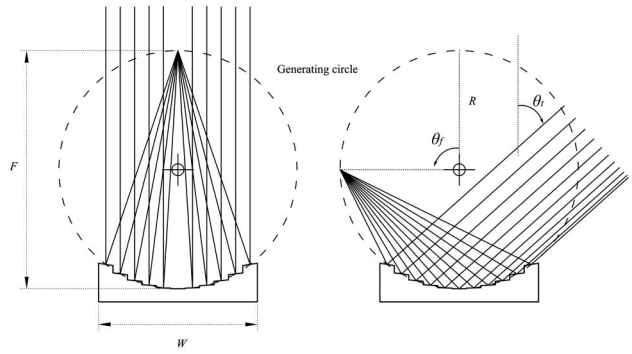


Fig. 2. Optical principle of the FMSC. The receiver moves along a circular path on the generating circle. The generating circle has a radius $R$, the focal length is $F = 2R$, and the receiver is positioned by the $\theta_f$ angle. The position angle of the receiver is twice the transversal incidence angle ($\theta_f = 2\theta_t$). The reflector width is $W$.

defined as the ratio of the focal length to the reflector width $F/W$, and the intercept factor $\gamma$ (defined as the fraction of the reflected radiation that is incident on the absorbing surface of the receiver [13]). See Fig. 3(a) for a visualization of the geometry. A standard evacuated tube with a flat fin was used as a receiver, as shown in Fig. 3(b).

From [10], it was concluded that as the number of mirrors increases, the optical efficiency decreases (due to the self-shadowing between the adjacent steps), and as the number of mirrors decreases, the radiation concentration on the receiver becomes smaller, and therefore heat losses become higher. On the other hand, a thermal study was carried out showing the net energy gained by the FMSC design for medium-range temperature applications [14]. Optimal designs of the FMSC were determined with the following parameter values: $\gamma = 0.98$, $N \geq 19$, and $F/W \geq 1.5$.

In the previous studies of the FMSC geometry [10,14], it was concluded that it is not possible to independently combine the two most relevant effects for maximizing useful energy in a solar concentrator: good optical performance and high concentration of radiation. Reducing one effect increases the other (good optical performance implies lower values of

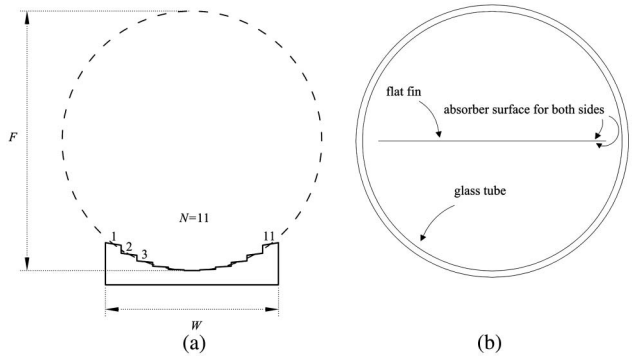


Fig. 3. (a) Schematic showing the focal length $F$, reflector width $W$, and number of mirrors $N$. (b) Front view of evacuated tube, where the tube is considered as a receiver.

$N$, and a high concentration of radiation implies high values of $N$). Russell *et al.* [6] showed that incorporating a secondary concentrator in the receiver minimizes its size, increasing the radiation concentration on the receiver and reducing thermal losses. However, the shadow generated by this secondary concentrator increases, causing a drop in the optical efficiency; hence, a decrease in the net useful energy was produced. Another possibility is to replace the flat mirrors by parabolic mirrors, which reflect sunlight to the same point for normal incidence. Hence, it is possible to combine the two effects mentioned above: one can minimize the size of the receiver (increasing the concentration) and simultaneously reduce the number of mirrors $N$ (improving the optical efficiency and reducing the effect of the reflector steps).

The FMSC design with parabolic mirrors has been referred to in the literature as the CSFMSC, and was first analyzed by Balasubramanian and Sankarasubramanian in 1993 [15]. The authors studied the CSFMSC using analytical geometric tools (similar to [6,7] in the 1970s), with the following considerations: infinitesimal mirrors (that is, a large number of curved mirrors), optical errors characterized by a Gaussian dispersion with $\sigma = 1.0$–$10.0$ mrad, and characterization of the angular size of the sun by a Gaussian distribution. The study showed that it was possible to achieve a geometric concentration ratio of $C_a = 7$ for a CSFMSC in front of a FMSC with a $C_a$ of 6.76 for $\sigma = 10$ mrad; however, for $\sigma = 2$ mrad, concentrations of $C_a = 21.3$ for a CSFMSC in front of a FMSC with a $C_a$ of 14.3 were obtained. Therefore, that study showed that it is possible to increase the concentration ratio by replacing infinitesimal flat mirrors with infinitesimal curved mirrors when the surface errors are sufficiently small.

In 2006, the authors of this paper performed a numerical study of the CSFMSC design with only one parabolic mirror ($N = 1$) using forward ray-tracing tools [16]. The optical efficiency was determined for different design parameters, but the specular reflection errors and the size of the sun were neglected.

For all of the above reasons and because of the current interest in the integration of solar collectors into building surfaces working within the temperature range between 100°C and 250°C [1], it would be of great interest to develop a methodology to determine the optical behavior of CSFMSCs (with a finite number of curved mirrors), with the aim of optimizing the solar radiation captured, depending on environmental conditions.

## 3. Physical Model

To generate the reflector geometry, beginning with the same assumptions adopted in [10], it was also assumed that the concentrator is symmetric, all the mirrors are of the same width, and the step walls are perpendicular to the central mirror. The total number of mirrors is $N$.

The mirrors are labeled from $i = 1$ to $n$ on the right-hand side of the generating circle because the reflector is symmetric ($N = 2n + 1$). The central points of the flat mirrors $(x_i, z_i)$ were determined in [10], and here, the central points of the parabolic mirrors are the same set of $(x_i, z_i)$ coordinates because the geometry is constructed by replacing the flat mirrors with parabolic mirrors.

The general equation of the parabola $z(x)$ in Cartesian coordinates, with a focal distance $c_3$, and a vertex in $x = c_1$, $z = c_2$, is given by

$$z(x) = \frac{(x - c_1)^2}{4c_3} + c_2. \tag{1}$$

To determine the cross section of the CSFMSC, it is necessary to know the $c_1$, $c_2$, and $c_3$ parameters for each parabolic mirror labeled with the subscript $i$: $c_{1,i}$, $c_{2,i}$, and $c_{3,i}$. Now, because it is assumed to be a symmetric reflector, the parameter $c_{1,i} = 0$. Then, $c_{2,i}$ and $c_{3,i}$ can be determined by solving the following system of equations:

$$z_i = \frac{x_i^2}{4c_{3,i}} + c_{2,i}, \tag{2}$$

$$2R = c_{3,i} + c_{2,i}. \tag{3}$$

Equation (3) implies the condition that all mirrors have the same focal point. Note that, for normal incidence, the receiver is positioned at the top of the circle and the focal length $F$ is equal to the diameter of the generating circle, $F = 2R$. As it was shown in [10], if we assume that the aperture of the concentrator is equal to 1, $W = 1$ u (where u is the unit of length), only two parameters are required to determine the concentrator's geometry: the number of mirrors, $N$, and the F-number, $F/W$. By solving Eqs. (2) and (3), we can construct the geometry of the reflector. Figure 4 shows the solution for the case of $N = 3$ and $F/W = 1.0$.

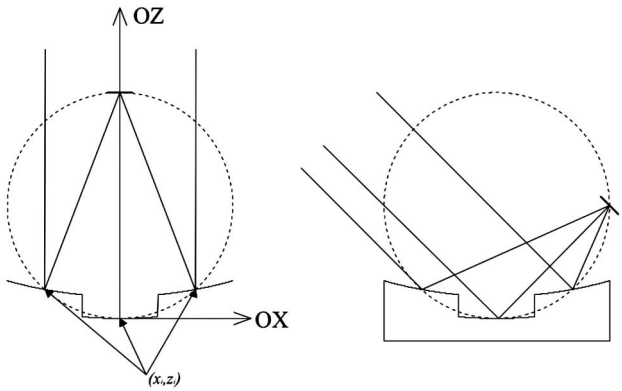


Fig. 4. CSFMSC reflector with $F/W = 1.0$, $N = 3$, and a geometric concentration of $C_a = 10$. A visualization of the principal rays is shown for normal incidence and for a 45° transversal incidence. The path of the receiver is the same as in the FMSC.

The size of the receiver was determined by the geometric concentration ratio, defined such that $C_a$ is the ratio of the reflector aperture size to the receiver aperture size. Then the width of the receiver is given by $a_r = 1/C_a$. Hence, the CSFMSC presented here is designed with the following three parameters: $N$, $F/W$, and $C_a$.

Figures 5 and 6 show a ray-tracing visualization of a CSFMSC design with parameters $N = 5$, $F/W = 1.0$, and $C_a = 10$. It can be observed that this design intercepts a large portion of the direct radiation, but when the incidence angle increases, the reflected radiation occupies a larger area, and some rays are lost. Note that the receiver intercepts the reflector when the sun is in the lower positions, and $\theta_{t,\mathrm{lim}}$ is the incidence transversal angle when the receiver intercepts the reflector. Then the receiver remains static for values greater than $\theta_{t,\mathrm{lim}}$ (see Fig. 6).

## 4. Cases Analyzed

Having taken into account the three design parameters that define the CSFMSC, the cases studied are the allowed combinations of the following parameter values:

- Number of mirrors, $N = 1, 3, 5, 7$
- F-number, $F/W = 1.0, 1.25, \ldots, 3.0$
- Geometric concentration ratio, $C_a = 3, 4, 5, 18, 20, \ldots, 30$

In this paper, 792 cases have been analyzed. The reason that cases with $N > 7$ have not been considered is because we want to reduce the number of mirrors with respect to the FMSC in order to find designs that are simpler from a manufacturing standpoint. Concerning the values of the geometric concentration ratio, the reason that cases with $C_a > 30$ have not been considered is because high losses are produced for off-axis sun positions (see Fig. 5). Note that the maximum value of 30 considered here is well below the maximum concentration ratio for a linear concentrator $C_{\max} = 212$ [13].

## 5. Forward Ray-Tracing Program

A forward ray-tracing code was implemented and was presented in [10]. In the ray-tracing program developed, the geometry of the solar concentrator

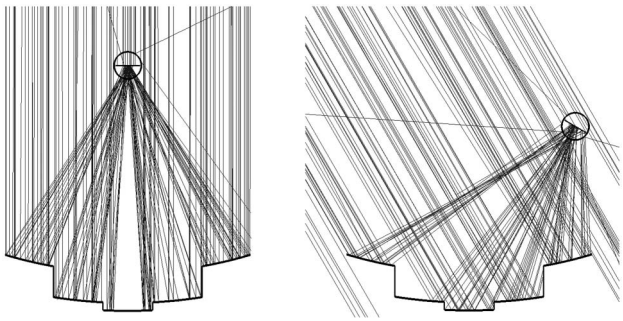

Fig. 5. CSFMSC with five parabolic mirrors ($N = 5$) and with parameters $F/W = 1.0$ and $C_a = 10$. A ray-tracing visualization is shown for transversal incidence angles $\theta_t = 0°$ and $\theta_t = 30°$.

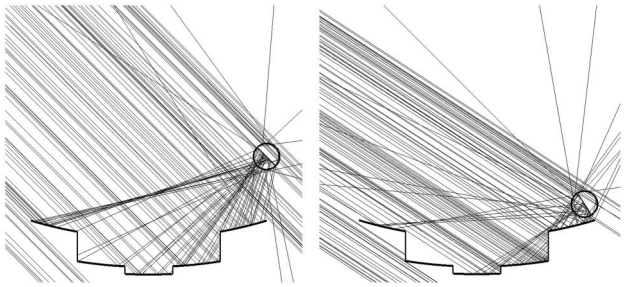

Fig. 6. CSFMSC with five parabolic mirrors ($N = 5$) and with parameters $F/W = 1.0$ and $C_a = 10$. A ray-tracing visualization is shown for transversal incidence angles $\theta_t = 45°$ and $\theta_t = 57°$. The last one corresponds to the angle limit of the receiver position $\theta_{f,\mathrm{lim}} = 114°$ when the receiver intercepts the reflector. In this case, for greater values of $\theta_t \geq \theta_{t,\mathrm{lim}} = 57°$, the receiver remains fixed at $\theta_{f,\mathrm{lim}} = 114°$.

is described by discrete elements with triangular surfaces. Four kinds of surfaces can be introduced: specular surfaces, opaque surfaces, interface surfaces (to model pieces of glass), and absorber surfaces (the receiver). The program calculates ray trajectories from one source (called the sun window) that emits to all the surfaces of the system, and only ray-optics propagation is taken into account. The angular size of the sun is modeled according to the Buie equations [17], and Fresnel effects are handled using a Monte Carlo approach. The program can calculate the optical efficiency and the radiation distribution on the absorber. The four types of material surfaces, the angular size of the sun, and the intersection detection algorithm were described in [10].

In a solar concentrator, the power absorbed by the receiver is given by [13]

$$S = G_b(\gamma\rho\tau\alpha)_0 K_{\gamma\rho\tau\alpha}, \tag{4}$$

where $G_b$ is the beam solar radiation on the reflector plane, $\gamma$ is the intercept factor (defined as the fraction of the reflected radiation incident upon the absorbing surface of the receiver), $\rho$ is the reflection coefficient, $\tau$ is the cover transmittance, $\alpha$ is the absorption coefficient, and $K_{\gamma\rho\tau\alpha}$ is the IAM. The 0 subscript indicates normal incidence. Ray-tracing is the most appropriate method for calculating the optical behavior of the CSFMSC, given its noncontinuous geometry and the multitude of forms that its design can take.

The same optical values as in [10] were used: the total reflectance of the mirrors $\rho = 0.92$; the angular dispersion on the mirrors $\sigma = 8$ mrad; the angular size of the sun characterized by the Buie equations [17] with a circumsolar ratio CSR = 0.05; the angular dependence on the incidence angle $\theta_i$ for the absorber surface according to Eq. (5) [18], where $\alpha_0 = 0.95$ is the normal absorptance; and the refraction coefficient of the glass tube, 1.56. For the dimensions of the evacuated tube, see [10].

$$\frac{\alpha}{\alpha_0} = 1 - 0.017\left(\frac{1}{\cos\theta_i} - 1\right)^{1.8}. \quad (5)$$

The IAM term $K_{\gamma\rho\tau\alpha}$ provides a performance factor to account for situations when the sun is not perpendicular to the collector. The IAM is then given by Eq. (6) for the perpendicular direction and Eq. (7) for the parallel direction:

$$K(\theta_t, 0) = \frac{\eta(\theta_t, 0)}{\eta(0, 0)}, \quad (6)$$

$$K(0, \theta_l) = \frac{\eta(0, \theta_l)}{\eta(0, 0)}, \quad (7)$$

where $\eta(0, 0)$ is the optical efficiency for normal incidence and is calculated by the ray-tracing program. See Fig. 1 for the definitions of the projection angles.

## 6. Results and Discussion

In this section, the optical efficiency at normal incidence, the transversal and longitudinal IAM curves, the goodness of the IAM factorization, and the local flux concentration on the absorber surface are analyzed. A convergence analysis was conducted before each numerical experiment in order to determine the minimum number of rays that needed to be computed in the ray-tracing to obtain a variability of the results lower than 0.005.

### A. Optical Efficiency at Normal Incidence

The optical efficiency for normal incidence is plotted in Fig. 7(a) for all cases studied. Simulations were performed with 200 000 random rays for each case. Maximum efficiency is achieved when the concentration is minimal, $C_a = 3$, taking values between 0.81 and 0.82. It was observed that as the concentration increases, the optical efficiency at normal incidence decreases. This is because the size of the receiver is smaller when $C_a$ increases, and therefore more reflected rays are lost due to the specular dispersion of the reflector. On the other hand, there is a strong dependence on the F-number $F/W$ parameter; as $F/W$ decreases, the optical performance increases. Note that, typically, the optical efficiency does not depend on the number of mirrors.

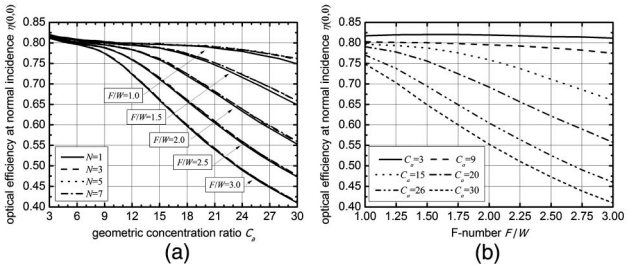


Fig. 7. (a) Optical efficiency at normal incidence as a function of the geometric concentration ratio for different values of F-number ($F/W$) and $N$. (b) Optical efficiency at normal incidence as a function of the F-number for $N = 1$.

The optical efficiency for normal incidence is plotted in Fig. 7(b) as a function of the F-number (only the case of $N = 1$ has been plotted because the other cases are quite similar [see Fig. 7(a)]). It can be seen that increasing the F-number produces a reduction in the optical efficiency. This is because an increase in the F-number causes the focal distance to increase, and therefore more rays do not reach the receiver because of the angular dispersion on the mirrors. Note also that this reduction is more pronounced for a small receiver (with high values of $C_a$), so low values of the F-number are needed to achieve high geometric concentration ratios. Nevertheless, the optical efficiency at normal incidence is not the only indicator involved in the optical behavior of the system, as the global optical efficiency is given by the product of $\eta(0, 0)$ and the IAM terms that are discussed below.

Due to the optical principle on which the CSFMSC is based (see Fig. 2), values of $F/W < 1$ are not of practical interest, in contrast to parabolic trough collectors, which typically have $F/W$ values in the range of 0.2–0.6 [19–21].

### B. Transversal IAM

Simulations were performed with 200 000 random rays for each transversal sun position in the range of 0°–80° in 1° steps. The simulations were performed in 3D, and the longitudinal incidence angle was assumed to be 0°. Due to the large number of cases calculated, in Figs. 8–10, only a few selected results have been shown in order to show the effects of such parameters on the transversal IAM. In Fig. 8, the effects of the $F/W$ parameter can be seen. It can be observed that increasing the $F/W$ value improves the transversal IAM curve. Note also that in some cases the curve takes a value that is greater than 1; this is because some of the radiation goes directly to the receiver without being reflected by the mirror and, thus, more energy can be captured than reaches the reflector aperture. In Fig. 9, the effect of the

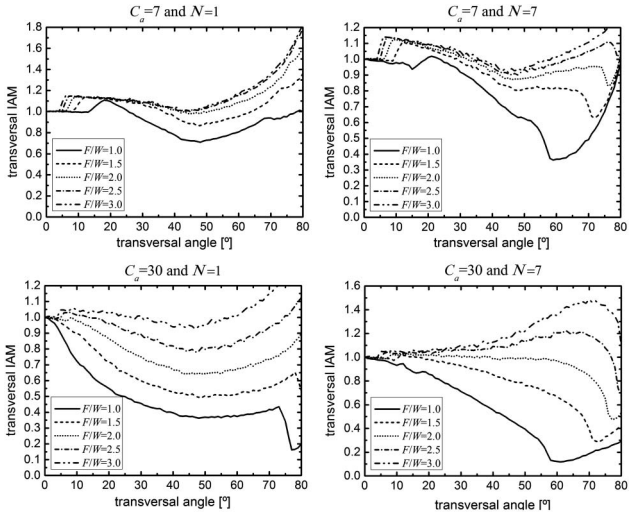


Fig. 8. Transversal IAM curves depending on the $F/W$ ratio as a function of transversal angle for different $C_a$ and $N$ values.

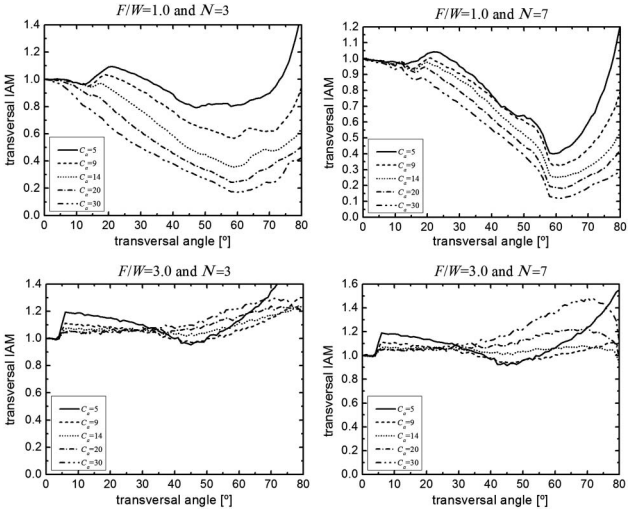


Fig. 9. Transversal IAM curves depending on the geometric concentration ratio as a function of the transversal angle for different $F/W$ and $N$ values.

concentration $C_a$ is analyzed; two different patterns can be seen. The first shows that increasing the concentration causes the transversal IAM to decrease, which is due to the fact that increasing $C_a$ decreases the size of the receiver, and therefore a portion of the reflected radiation does not reach the receiver. This pattern occurs for low $F/W$ values. The second pattern, which occurs for high $F/W$ values, inverts this tendency when radiation goes directly to the receiver without being reflected by the mirror. This is because the effect of ray interception in the steps is low for a high $F/W$ value, and in this scenario, more energy is captured with respect to the case of normal-incidence radiation. Finally, in Fig. 10, the effect of the number of mirrors is analyzed. In this case, there is no uniform pattern, as variations of the parameters $F/W$ and $C_a$ significantly change the optical response to variations in the number of mirrors $N$.

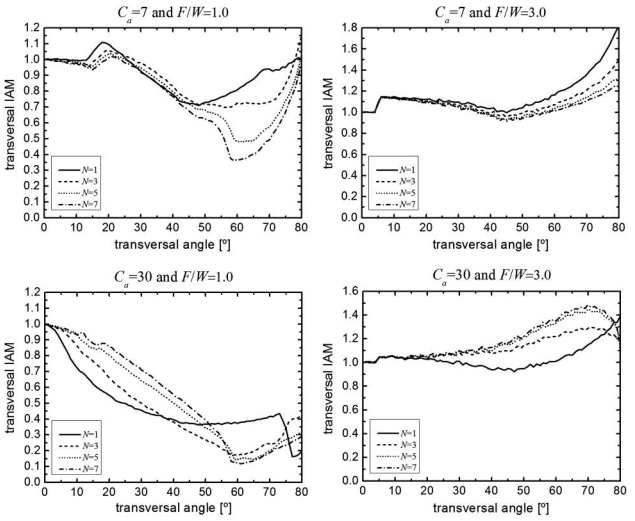


Fig. 10. Transversal IAM curves depending on the number of mirrors as a function of the transversal angle for different $C_a$ and $F/W$ values.

## C. Longitudinal IAM

To calculate the longitudinal IAM, it was assumed that the length of the concentrator in the longitudinal dimension was $L = 10$ u. Simulations were performed with 400 000 rays for each of the longitudinal angles from 0° to 80° in 1° steps. Figure 11 shows the dependence of the longitudinal IAM on the longitudinal angle and other parameters. In Fig. 11, it can be observed that increasing the $F/W$ value produces a reduction of the longitudinal IAM values. This is because an increase in $F/W$ causes an increase in the distance between the reflector and the receiver, and therefore more rays do not reach the receiver and tip losses increase. For the geometric concentration $C_a$, it can be seen that increasing $C_a$ also produces a reduction in the longitudinal IAM values. This is because an increase in $C_a$ causes the size of the receiver $a_r$ to decrease, and a small receiver captures less energy. Finally, the effect of the number of mirrors $N$ is analyzed. It can be observed that its effects are almost negligible in all cases studied.

## D. Factorization Approximation for the IAM

It has been suggested that the IAM $K$ for low-concentration collectors could be factorized according to $K \sim K(\theta_t, 0)K(0, \theta_l)$ [11]. Nevertheless, the use of a factorized IAM can cause errors in the estimation of the energy collected [22]. In order to perform a complete optical study of the CSFMSC, as was done in [10] for the FMSC, to find out how reliable the factorization approximation for the IAM is, the

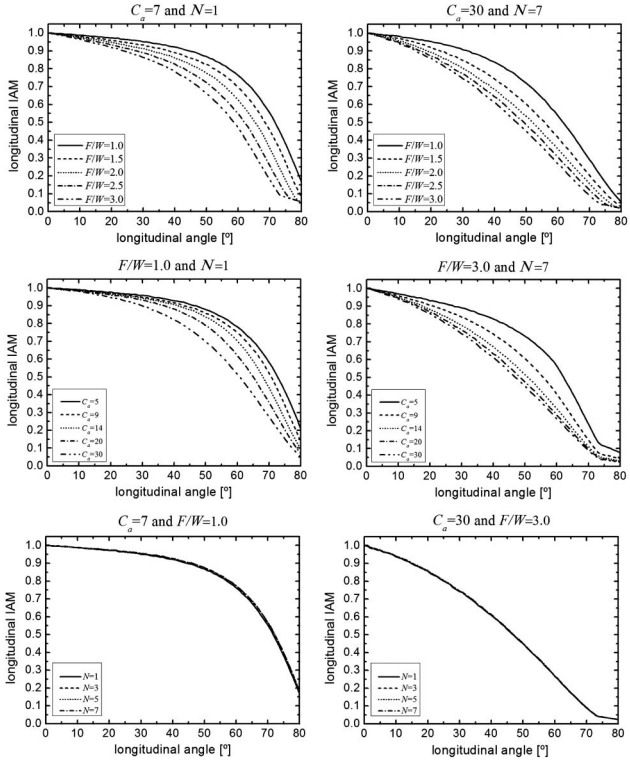


Fig. 11. Longitudinal IAM curves for various values of $F/W$, $C_a$, and $N$.

IAM calculated with this approximation was compared with a 3D ray-tracing analysis for 160 randomly chosen cases of the 792 cases studied. The IAM calculated by the ray-tracing corresponds to the zenith and azimuth angles between 0° and 90° in 5° steps. Then, for each pair of values, a transformation is applied in order to obtain the IAM calculated by ray-tracing as a function of the transversal and longitudinal angles $K(\theta_t, \theta_l)$. Simulations were performed with 400 000 rays. The error between the approximation and the theoretical value is given by Eq. (8); the cosine factor $\cos(\theta_i)$ is required to reference the error to the case of perpendicular beam irradiance

$$\Delta K = [K(\theta_t, 0)K(0, \theta_l) - K(\theta_t, \theta_l)]\cos(\theta_i). \quad (8)$$

Four error estimators were used to assess the goodness of the factorization approximation: the root mean square error (RMSE), the mean bias error (MBE), the mean absolute error (MAE), and the mean error (ME). The following equations give the expressions for each error estimator:

$$\mathrm{RMSE} = \left[\frac{1}{N_p}\sum \Delta K^2\right]^{1/2}, \quad (9)$$

$$\mathrm{MBE} = \frac{1}{N_p}\sum \Delta K, \quad (10)$$

$$\mathrm{MAE} = \frac{1}{N_p}\sum \frac{|\Delta K|}{K(\theta_t, \theta_l)\cos(\theta_i)}, \quad (11)$$

$$\mathrm{ME} = \frac{1}{N_p}\sum \frac{\Delta K}{K(\theta_t, \theta_l)\cos(\theta_i)}. \quad (12)$$

The average value of each of these estimators was calculated for angles from 0° to 70° for the 160 random cases. Table 1 reports the averages of RMSE, MBE, MAE, and ME. Based on the results, the factorized approximation provides an underestimation of the energy collected, as can be seen from the negative values in MBE and ME. It is reasonable to assume that this underestimation of captured energy is caused by an overestimation of the tip losses. Simple factorization assumes that the receiver is always positioned at the highest position of the circle, which is not a realistic assumption. To overcome this effect, the longitudinal IAM factor can be modified according to a simple geometrical analysis, which gives the correction factor $f(\theta_t, \theta_l)$ described in Eq. (13) (the same term as proposed for the FMSC in [10]), where $L$ is the length of the concentrator in the longitudinal dimension and $\theta_{t,\mathrm{lim}}$ is the transversal incidence angle when the intersection between the receiver and the reflector occurs. $f(\theta_t, \theta_l)$ is 1 when the longitudinal angle is greater than 75° in order to avoid singularity when the angles reach 90°. The new factorization is $K \sim K(\theta_t, 0)K(0, \theta_l)f(\theta_t, \theta_l)$.

**Table 1. Averages of Error Estimators for Comparison of the Factorized IAM and Ray-Tracing IAM**

| $\mathrm{IAM}_{\mathrm{Approximation}}$ | RMSE | MBE | MAE(%) | ME(%) |
|---|---|---|---|---|
| $K(\theta_t, 0)K(0, \theta_l)$ | 0.0354 | −0.0169 | 5.31 | −4.82 |
| $K(\theta_t, 0)K(0, \theta_l)f(\theta_t, \theta_l)$ | 0.0214 | −0.0028 | 3.14 | −1.26 |

$$f(\theta_t,\theta_l) = \begin{cases} \frac{L-[R+R\cos(2\theta_t)]\tan(\theta_l)}{L-2R\tan(\theta_l)} & \theta_t < \theta_{t,\mathrm{lim}} \text{ and } \theta_l < 75 \\ \frac{L-[R+R\cos(2\theta_{t,\mathrm{lim}})]\tan(\theta_l)}{L-2R\tan(\theta_l)} & \theta_t \geq \theta_{t,\mathrm{lim}} \text{ and } \theta_l < 75 \\ 1 & \theta_l \geq 75 \end{cases}, \quad (13)$$

With the new factorization, the values of RMSE, MBE, MAE, and ME decreased, and there was no longer a clear underestimation of the IAM, as can be seen in Table 1. In Fig. 12(a), the proposed factorization and theoretical IAM are plotted for the case that has the maximum MAE and ME values of the 160 random cases; it can be seen that the two plots

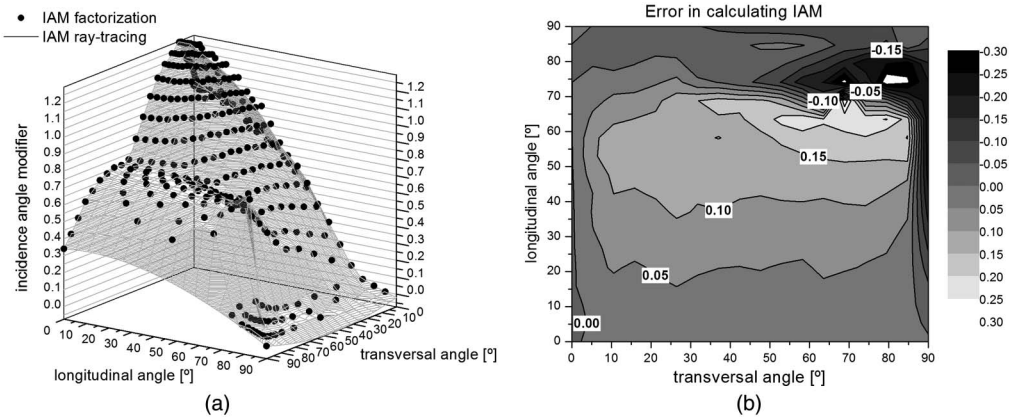


Fig. 12. Analysis of the case of $N = 1, F/W = 3.0$, and $C_a = 3$. (a) Factorized IAM, calculated by ray-tracing. (b) Error in the calculation of the energy collected from direct radiation if $K \sim K(\theta_t, 0)K(0, \theta_l)f(\theta_t, \theta_l)$ is used instead of $K(\theta_t, \theta_l)$. The values of the error estimators are RMSE = 0.0615, MBE = −0.0206, MAE = 7.68%, and ME = 7.55%.

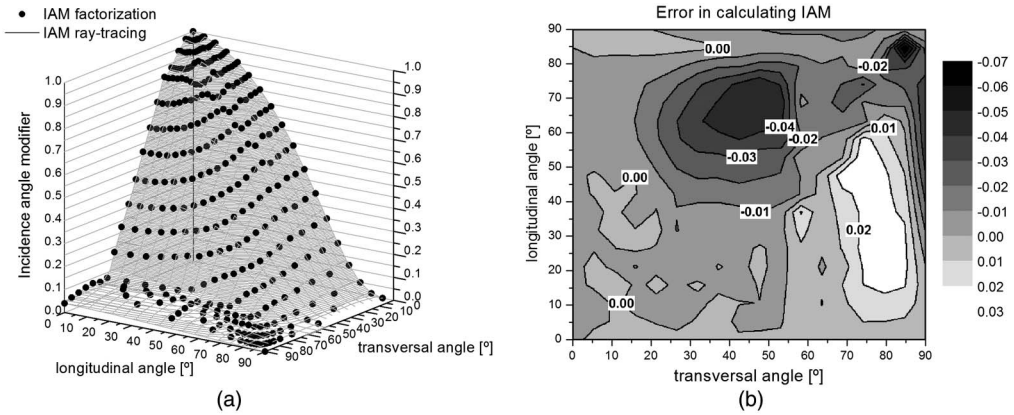


Fig. 13. Analysis of the case of $N = 7, F/W = 1.0$, and $C_a = 24$. (a) Factorized IAM, calculated by ray-tracing. (b) Error in the calculation of energy collected from direct radiation if $K \sim K(\theta_t, 0)K(0, \theta_l)f(\theta_t, \theta_l)$ is used instead of $K(\theta_t, \theta_l)$. The values of the error estimators are RMSE = 0.0109, MBE = −0.0035, MAE = 3.47%, and ME = −1.38%.

are quite similar. In Fig. 12(b), the $\Delta K$ error is plotted. The large error peaks are produced for very high angles in both transversal and longitudinal directions. Hence, the factorized approach does not reproduce the real value of the IAM for high values of $\theta_t$ and $\theta_l$. However, these errors do not have a significant effect on the estimate of the energy captured, as the errors occur at angles where the incident energy on the concentrator plane is quite small, and moreover, the IAM value is extremely low. It can be observed for this case that in the range of $0 \le \theta_t \le 80 \cap 0 \le \theta_l \le 40$ the error between the factorized IAM and the ray-tracing IAM was less than 0.1. Another case is shown in Figs. 13(a) and 13(b), with values of RMSE, MBE, MAE, and ME similar to the average values of the 160 random cases analyzed. An error less than 0.04 is produced over a large range of the possible values of $\theta_t$ and $\theta_l$.

### E. Radiation Distribution on the Absorber

The dependence of the concentration of radiation on the local receiver position has been calculated for four design cases and three incidence transversal angles: $\theta_t = 0°$, 30°, and 60°. The ray-tracing program simulates $10^6$ rays for each transversal angle, and the receiver has been discretized into 100 cross

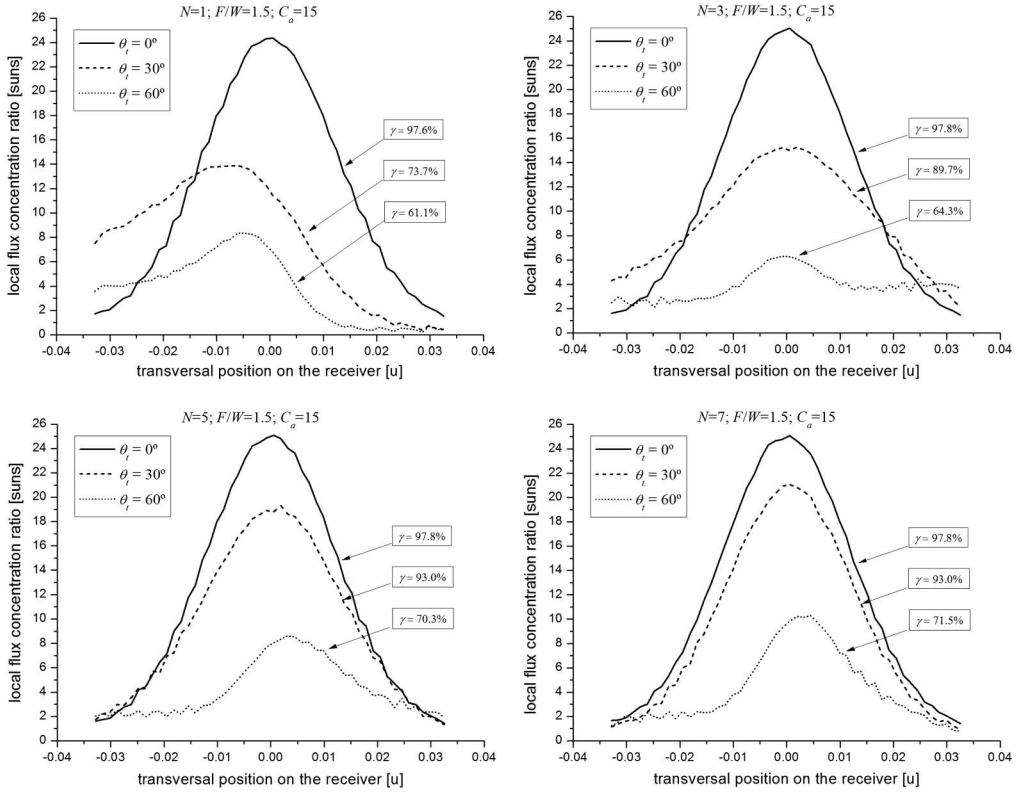


Fig. 14. Local distribution of the radiation on the receiver for $N = 1, 3, 5$, and 7 for $F/W = 1.5$ and $C_a = 15$. The longitudinal length of the concentrator was considered to be $L = 1$ u.

sections. The results are shown in Fig. 14. The units are given in suns, which corresponds to the radiation density of the direct normal irradiation (DNI). We analyzed the following designs: $N = 1$, 3, 5, and 7 for $F/W = 1.5$ and $C_a = 15$. It was observed that the concentration of radiation at normal incidence ($\theta_t = 0°$) is symmetric irrespective of the number of mirrors. It is also observed that the fraction of energy intercepted by the receiver (called $\gamma$) reaches nearly 98% regardless of the number of mirrors. The maximum concentration, which is around 25 suns, is also achieved regardless of the number of mirrors. In all cases it is observed that the concentration of radiation decreases with an increasing angle of solar incidence, as expected.

For the case of one parabolic mirror, $N = 1$, there are higher energy losses as the angle of incidence increases, showing high-concentration values of eight suns for $\theta_t = 30°$ in the tail of the bell curve. For three parabolic mirrors, substantially improved energy is captured with respect to the case of a single mirror, but also optical losses in the tails of the bell curve are produced. The cases of five and seven parabolic mirrors both have a similar radiation distribution, and almost all the energy from the mirrors is intercepted by the receiver. The fact that high values of the interception factor $\gamma$ are not reached in these cases is due to the interception of reflected rays by the steps, which can be estimated to cause a loss of ≈30% for $\theta_t = 60°$. Finally, increasing the angle of incidence increases slightly the asymmetry in the distribution of radiation on the receiver where the peak is displaced from the center.

## 7. Conclusions

An optical analysis of the CSFMSC design has been conducted for $F/W$ ratios ranging from 1 to 3, for geometric concentration ratios $C_a$ ranging from 3 to 30, and for a number of mirrors $N$ ranging from 1 to 7. The optical performance of the CSFMSC with an average concentrator quality characterized by $\sigma = 8$ mrad has been fully characterized between those ranges.

A maximum optical efficiency at normal incidence of 82% could be reached, but it decreased when the concentration increased. The best optical performance at normal incidence is achieved for $F/W = 1$. The CSFMSC design has been characterized optically, and the transversal and longitudinal IAM curves have been determined. It has been shown that any given parameter can affect the transversal and longitudinal IAM curves in different ways. Large $F/W$ ratios have a negative effect on the transversal and longitudinal IAM. Variations of $C_a$ and $N$ have different effects on the transversal IAM curves. An increase of the concentration $C_a$ negatively affects the longitudinal IAM. Changing the number of mirrors $N$ does not significantly affect the longitudinal IAM.

The same analytic term added in the factorized approximation in the IAM for the FMSC in [10] has been evaluated for the CSFMSC in this paper. Although this approximation does not reproduce the IAM value for high incidence angles, it can be assumed that it does not have a significant effect on the estimate of the energy captured as it occurs at angles where the incident energy on the concentrator aperture area is quite small, and the corresponding IAM value is extremely low.

The local flux radiation has been analyzed, and it has been observed that, for the case of one parabolic mirror $N = 1$, large losses are produced when the incident transversal angle increases.

Although a complete thermal analysis is required to determine the optimal geometry for any given application, the most promising geometries for the use of the CSFMSC in medium-range temperatures (100°C–250°C) appear to be those with $F/W$ factors between 1 and 2, which can provide geometric concentration ratios in the range of 5–15 with acceptable optical efficiencies and IAM curves. These cases have better optical behavior than the corresponding FMSC cases, resulting in a concentrator with fewer reflector segments for the same concentration and optical efficiency.

This work was co-funded by the Ministerio de Educación y Ciencia del Gobierno de España (project number CIT-12000-2007-38), the Universitat de les Illes Balears, and Tecnología Solar Concentradora, S.L. We thank them all heartily.

## References

1. IEA, "Technology roadmap: solar heating and cooling" (2012).
2. J. M. Gordon and M. Jeffrey, *Solar Energy the State of the Art: ISES Position Papers* (James & James, 2001).
3. W. G. Steward and F. Kreith, "Stationary concentrating reflector cum tracking absorber solar energy collector: optical design characteristics," Appl. Opt. **14**, 1509–1512 (1975).
4. M. F. El-Refaie, "Performance analysis of the stationary-reflector/tracking-absorber solar collector," Appl. Energy **28**, 163–189 (1987).
5. M. F. El-Refaie, "Performance analysis of the stationary-reflector/tracking-absorber solar collector," Energy Convers. Manag. **29**, 111–127 (1989).
6. J. L. Russell, E. P. DePlomb, and R. K. Bansal, "Principles of the fixed mirror solar concentrator," 139–145 (1974).
7. R. L. Bansal, "Theoretical analysis of fixed mirror solar concentrator," Ph.D. thesis (Arizona State University, 1974).
8. G. H. Eggers and J. L. Russell, "The FMSC collector subsystem for the Sandia Solar Total Energy Facility," in *Solar Cooling and Heating: Architectural, Engineering, and Legal Aspects; Proceedings of the Forum* (Hemisphere Publishing, 1978), pp. 255–271.
9. V. E. Dudley and R. M. Workhoven, "Summary report: concentrating solar collector test results: Collector Module Test Facility (CMTF). January–December 1978," SAND78-0977 (1979).
10. R. Pujol Nadal and V. Martínez Moll, "Optical analysis of the fixed mirror solar concentrator by forward ray-tracing procedure," J. Sol. Energy Eng. **134**, 031009 (2012).
11. W. R. McIntire, "Factored approximations for biaxial incident angle modifiers," Sol. Energy **29**, 315–322 (1982).
12. D. Chemisana, A. Coronas, J. López-Villada, J. I. Rosell, and C. Lodi, "Building integration of concentrating systems for solar cooling applications," Appl. Therm. Eng. **50**, 1472–1479 (2013).
13. J. A. Duffie and W. Beckman, *Solar Engineering of Thermal Processes* (Wiley, 1991).

14. R. Pujol Nadal, "Comportamiento óptico y térmico de un concentrador solar lineal con reflector estacionario y foco móvil," Ph.D. thesis (University of Balearic Islands, 2012), http://hdl.handle.net/10803/84115.
15. V. Balasubramanian and G. Sankarasubramanian, "Stretched tape design of fixed mirror solar concentrator with curved mirror elements," Sol. Energy **51**, 109–119 (1993).
16. V. Martínez Moll, R. Pujol Nadal, A. Moià Pol, and H. Schwiger, "Analysis of a stationary parabolic linear concentrator with tracking absorber," in *13th International Symposium on Concentrated Solar Power and Chemical Energy Technologies* (2006).
17. D. Buie, C. J. Dey, and S. Bosi, "The effective size of the solar cone for solar concentrating systems," Sol. Energy **74**, 417–427 (2003).
18. T. Tesfamichael and E. Wäckelgård, "Angular solar absorptance of absorbers used in solar thermal collectors," Appl. Opt. **38**, 4189–4197 (1999).
19. A. Rabl, P. Bendt, and H. W. Gaul, "Optimization of parabolic trough solar collectors," Sol. Energy **29**, 407–417 (1982).
20. A. Fernández-García, E. Zarza, L. Valenzuela, and M. Pérez, "Parabolic-trough solar collectors and their applications," Renew. Sust. Energ. Rev. **14**, 1695–1721 (2010).
21. G. Zhu, "Study of the optical impact of receiver position error on parabolic trough collectors," J. Sol. Energy Eng. **135**, 031021 (2013).
22. M. Rönnelid, B. Perers, and B. Karlsson, "On the factorisation of incidence angle modifiers for CPC collectors," Sol. Energy **59**, 281–286 (1997).